PSFC/JA-04-2

High-field side scrape-off layer density profiles inferred from D_α emission on Alcator C-Mod

C. J. Boswell, J. L. Terry, B. LaBombard, B. Lipschultz, C. S. Pitcher

Plasma Science and Fusion Center
Massachusetts Institute of Technology
Cambridge, MA 02139

Feb 2004

Submitted to: Plasma Physics and Controlled Fusion

This work was supported by the U. S. Department of Energy Contract No. DE-FC02-99ER54512. Reproduction, translation, publication, use and disposal, in whole or in part by or for the United States government is permitted.

High-field side scrape-off layer density profiles inferred from D-alpha emission on Alcator C-Mod

C J Boswell, J L Terry, B LaBombard, B Lipschultz, and C S Pitcher

Plasma Science and Fusion Center, Massachusetts Institute of Technology, Cambridge, MA 02139

E-mail: boswell@psfc.mit.edu

Abstract. Measurements from an inner wall mounted scanning Langmuir probe and modelling of D_α emission show a sharp fall-off of plasma density in the inboard private flux region. D_α emission is modelled using a one dimensional space, two dimensional velocity kinetic neutral code in order to track the changes in the density profile while the magnetic topology is changed from single to double null. A sharp density decay is observed to track with the location of the secondary separatrix. The presented data is consistent with a lower level of cross-field transport on field lines in the private flux region restricted to the high-field side when compared to cross-field transport on field lines in the low-field side scrape-off layer.

1. Introduction

The study of scrape-off layer (SOL) characteristics and behaviour has been primarily based on the studies of the outer (low field side) SOL. One reason for this emphasis is the diagnostic access to the outer SOL. Due to the geometry of a tokamak it is much simpler to measure the plasma parameters on the low field side of the plasma where there is nothing obstructing the access to the plasma. Whereas, to make measurements of the inner (high field side) SOL either the hot core plasma is in the way or the diagnostic must be mounted on the inner wall where there are higher magnetic fields and less mounting space than that on the outer edge of the tokamak.

Although studies of the inboard SOL have been few, they have noted significant differences between the inner SOL and the outer SOL. On Alcator C [1] (a limited tokamak) it was noted that there was a poloidal variation of density in the shadow of the limiter with the minimum occurring on the high-field-side. Another result from that same study was that the radial density e-folding length also had a minimum value on the inner SOL, with the maximum occurring on the outer SOL. A result from the ASDEX tokamak [2] (a diverted tokamak) is that fluctuations typical of the low-field-side SOL would be observed on the high-field-side SOL when in a single null discharge, but when in a balanced double null discharge the fluctuations were absent from the high-field-side SOL. A study on TEXT-U [3] compared turbulence characteristics on the inboard and outboard edges and found that for diverted discharges the fluctuations on the inboard side "were too small to be measured by the diagnostic, demonstrating that the source of the turbulence may be localized to the outboard edge." Similar observations and conclusions were made on Alcator C-Mod [4], where normalised fluctuation levels on the inboard side were found to be typically 5-10 times lower than on the outboard side of the same flux surface. The frequency spectra were also quite different.

Using a CCD camera filtered for D_α emission viewing the inner SOL tangentially is one way to measure these transport properties directly. The data from a CCD camera can be used to augment the data collected from a scanning Langmuir probe mounted t the inner wall to allow for the calculation of neutral density profiles. A CCD camera also provides a large poloidal coverage allowing for the ability to track two dimensional changes (i.e., as magnetic topology is changed) as a function of time. The camera also directly provides information on fuelling source locations. All of these capabilities are have been used to study differences between the inner and outer SOL transport.

Section 2 presents scanning Langmuir probe measurements showing a sharp density fall-off at the secondary separatrix on the high-field side SOL and corresponding D_α profiles. Section 3 discusses the modelling of neutral transport and D_α emission to yield density profile information directly from D_α measurements. And section 4 provides the conclusions and summary of the presented results and analysis.

2. Measurements

The first set of measurements shown involves a scanning Langmuir probe mounted to the inner wall of Alcator C-Mod. This scanning probe has a similar design to that developed and employed at ASDEX Upgrade [5] and to the divertor bypass system installed on Alcator C-mod [6]. Both of these systems use the toroidal magnetic field

and a solenoid coil to provide the torque required to swing the probe or divertor bypass flaps. The second measurements are of the D_α brightness in the region near the inner wall. These measurements are recorded using a tangentially viewing CCD camera filtered for D_α emission [7].

All presented measurements were taken in a near double null magnetic configuration. In this configuration there exists three distinct flux regions in the SOL (shown in figure 1): 1) a private flux region (inner SOL) where the flux surfaces do not connect to the low-field-side SOL (shown in green in figure 1) and bounded by the inner wall and the secondary separatrix, 2) another private flux region (outer SOL) where the flux surfaces do not connect to the high-field-side SOL (shown in light blue in figure 1) and bounded by the outer wall and the secondary separatrix, and 3) the common SOL where the the flux surfaces do connect between the high- and low-field-sides of the SOL (shown in orange in figure 1) and bounded by the secondary and primary separatrices.

2.1. Probe Measurements

The scanning Langmuir probe is a single tungsten wire in a carbon fibre body mounted at the mid-plane on the inner wall. The probe is mounted such that the wire is horizontal and has an axis in the vertical direction about which it rotations. The scanning motion is obtained by a solenoid whose placement and applied magnetic field, in conjunction with the toroidal magnetic field, applies a torque to the scanning probe allowing it to swing in the plasma by up to 1.5 cm. This probe is then used to obtain plasma temperature, density, and potential profiles of the inner wall region.

Figure 2 show a series of density profiles obtained by the inner wall scanning probe (ISP) compared to an outboard scanning probe (ASP) for different distances between the primary and secondary separatrices. The ASP is a linear scanning probe consisting of four Langmuir probes and mounted on the low field side of the tokamak and above the mid-plane by 10.9 cm. In all cases the electron density does have a stronger decay in the region between the secondary separatrix and the inner wall than between the secondary separatrix and the outer wall.

2.2. D_α Measurements

To observe the D_α emission from the inner wall region, a visible imaging CCD camera was used. [7] This camera views the inner wall tangentially. A poloidal cross-section of the view is shown in figure 1. The camera is filtered for D_α using an interference filter located directly in front of the lens and is absolutely calibrated. The camera is located $\sim$19.5 cm below the mid-plane of the tokamak and has a slight upward tilt of $\sim$5 degrees. This view was calibrated by fitting the observed spacings between the tiles on the inner column to the expected location of the spacings on the image plane.

Although in principle an Abel inversion can be performed using the array of pixels whose view lies in the horizontal plane, the pixel to pixel noise renders this approach impractical. To obtain emission profiles from this region, the brightness profile was fitted to a line-integrated brightness profile based on an assumed emission

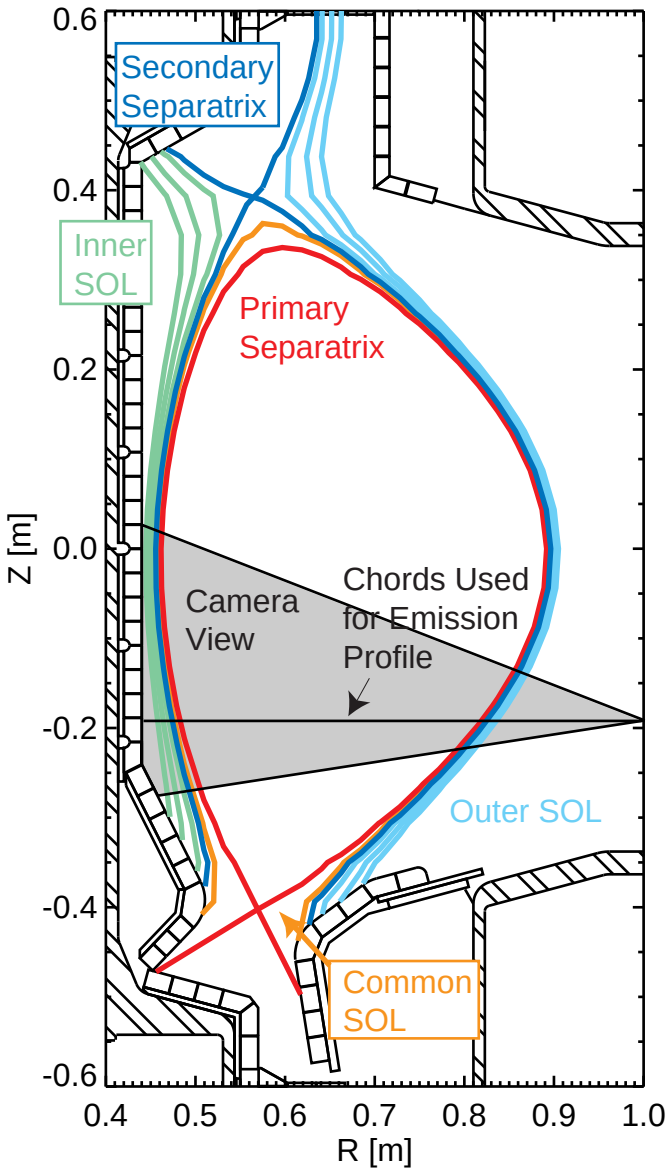

Figure 1. The inner (green), outer (light blue) and common scrape-off layer (orange) in a typical lower single null discharge, along with the poloidal projection of the camera view shaded (grey) and the chords used in determining the emissivity profile (solid horizontal line).

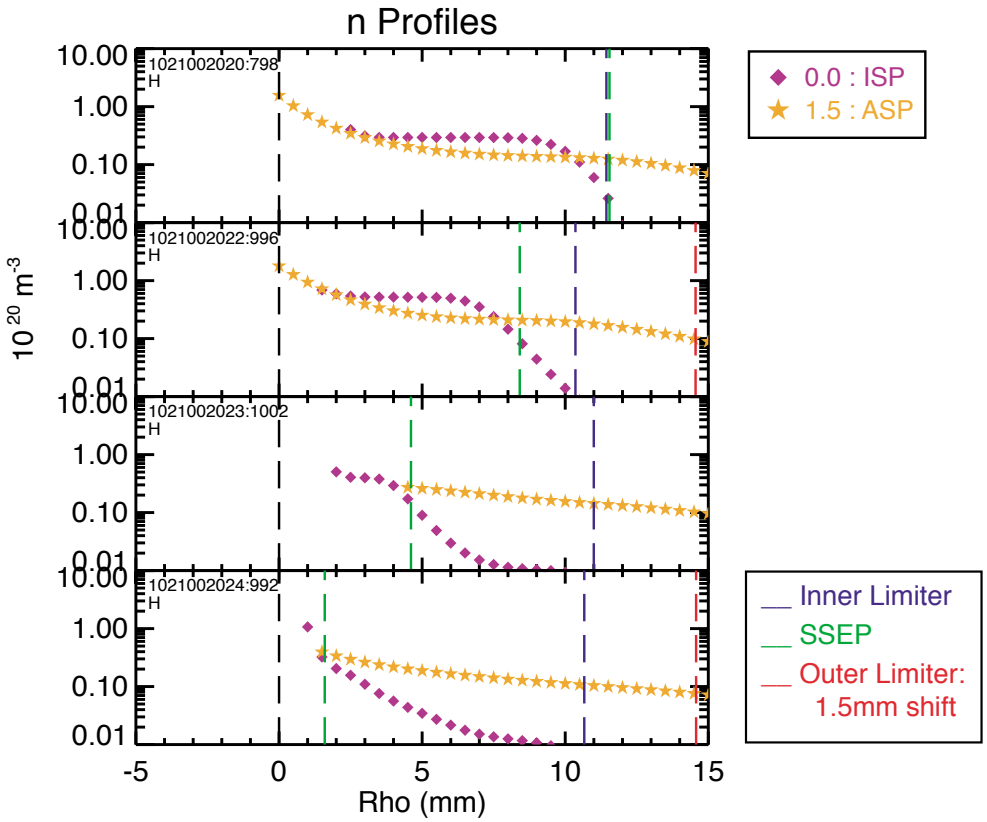

Figure 2. A series of density profiles mapped to the outboard mid-plane and plotted as a function of distance from the primary separatrix (ρ), where the primary separatrix is defined as being at $\rho = 0$. The profiles are the inner wall scanning probe (ISP) compared to an outboard scanning probe (ASP) for different distances between the primary and secondary separatrices. SSEP is the location of the secondary separatrix mapped to the outboard mid-plane.

profile shape. The emission profile was assumed to have the form,

$$\epsilon(r) = \begin{cases} c_0 \exp\left[\frac{r-r_0}{\lambda_-}\right] & \text{if } r \leq r_- \\ \epsilon_0 + c_1 (r-r_0)^2 & \text{if } r_- \leq r \leq r_+ \\ c_2 \exp\left[\frac{-r+r_0}{\lambda_+}\right] & \text{if } r_+ \leq r \end{cases} . \quad (1)$$

Figure 3 shows a sample emission based on equation 1. The variables r_0, r_-, and r_+ are the locations of the peak emission, the high-field-side boundary between the parabolic and exponential sections of the emission and the low-field-side boundary between the parabolic and exponential sections, respectively. The total number of free parameters can be reduced to 5 (i.e., ϵ_0, r_0, λ_-, λ_+, and c_2) by requiring that the function be differentiable at r_- and r_+.

The measured brightness profiles were fitted to the brightness profile of the assumed emission profiles including a constant brightness offset (presumably coming

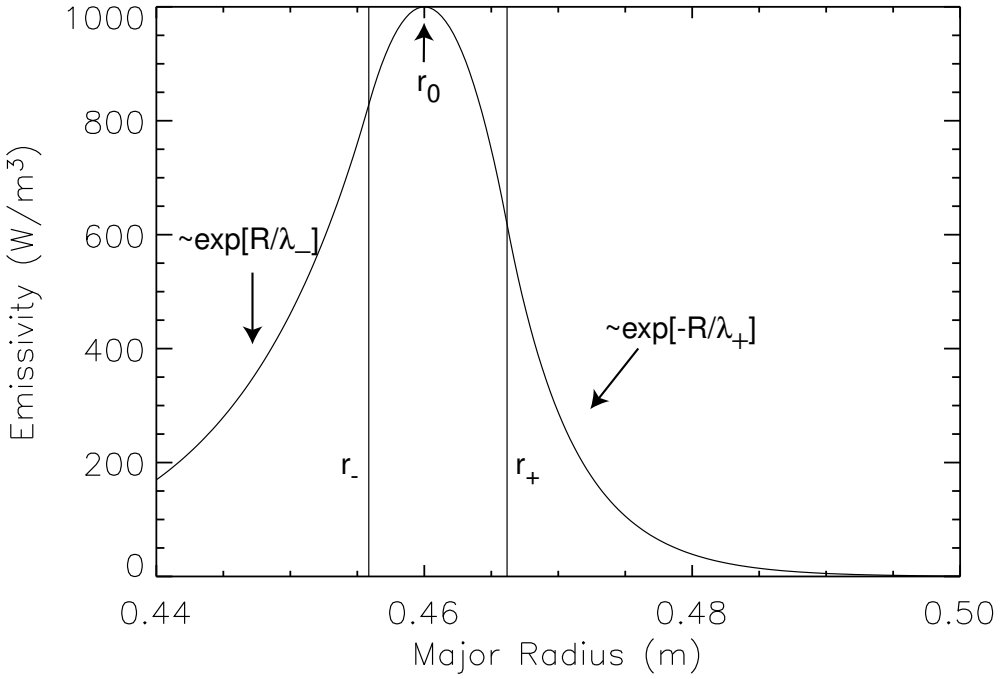

Figure 3. A sample of the emission profile assumed in the analysis of the D_α emission near the inner wall.

from the outer parts of the plasma through which the camera must view),

$$b(y) = 2\int_y^a \epsilon(r)\frac{r\ dr}{\left(r^2 - y^2\right)^{1/2}} + b_0. \tag{2}$$

Equation (2) with the differentiability at r_- and r_+ constraint has six free parameters, ϵ_0, the peak emission value, r_0, the location in radius of the emission peak, λ_-, the scale length of the emission toward the radial axis, λ_+, the scale length of the emission away from the radial axis, c_1, the "peakedness" of the emission, and b_0 the brightness offset. The constant brightness offset can be attributed to the twice brightness from the low-field side of the plasma, owing to the fact that the chords view the low-field-side of the plasma twice, once near the camera and another time on the far side of the tokamak. Figure 4 shows a typical brightness profile with the fitted function over-plotted. This fit can be done for all recorded frames.

To investigate the influence the magnetic geometry has on the D_α emission near the inner wall, the magnetic configuration was scanned dynamically from a lower single null (LSN) to a double null (DN) through to an upper single null (USN). Figure 5 shows the three configurations that the magnetic geometry was scanned through. The global parameters for this experiment were typical of an L-mode discharge on Alcator C-Mod and kept nearly constant: $B_T = 5.4$ T, $I_p = 0.8$ MA, $\bar{n}_e \approx 10^{20}$ m^{-3}. The main magnetic effect of this scan is the location of the secondary separatrix with respect to the primary separatrix, from ~ 1 cm from the primary separatrix at the outboard mid-plane to having no secondary separatrix during double null back to being ~ 1 cm from the primary separatrix with a change in the null with which the secondary separatrix is associated.

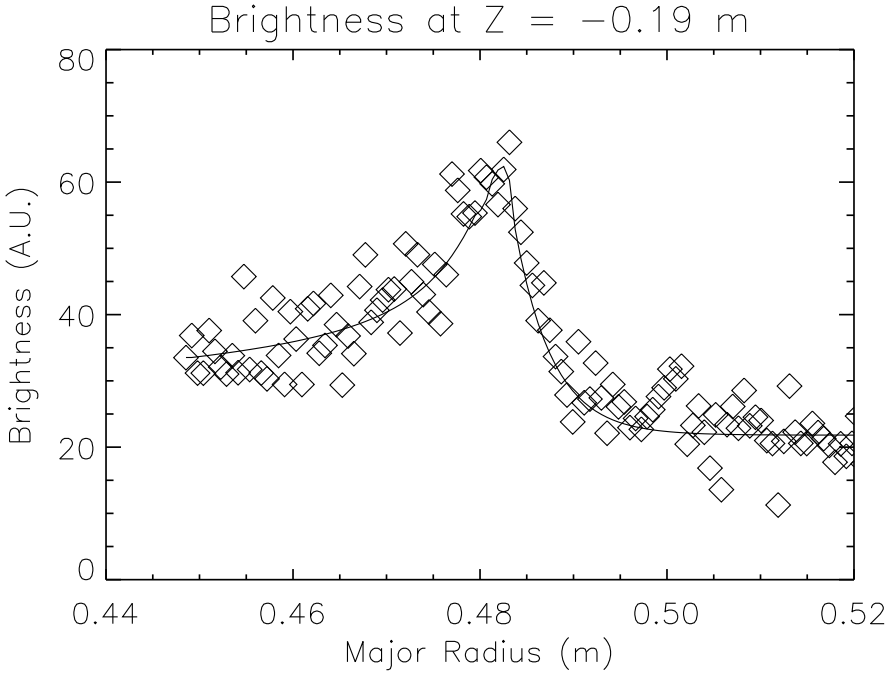

Figure 4. A typical brightness profile with the fitted function over-plotted. The abscissa is the major radius of the viewing chord's impact parameter.

By fitting the brightness profiles from the CCD camera, the variation of the location of the emissivity peak (r_0), the HFS emission scale length (λ_-), and the LFS emission scale length (λ_+) were determined for a discharge in which the magnetic geometry was scanned from a lower single null to an upper single null. The location of the emissivity peak during the configuration sweep is summaries in figure 6, and can clearly be seen to follow the secondary separatrix regardless of the null with which the secondary separatrix is associated. The HFS emission scale length, shown in figure 7, is relatively constant within the error of this measurement. The LFS emission scale length has a smaller error associated with its measurement and is systematically smaller when the discharge is near double null configuration. The LFS emission scale length measurements are summaries in figure 8.

3. Discussion

All three of these observations can be explained by a steep plasma density decay beginning at the secondary separatrix and decaying toward the inner wall and a relatively flat plasma density profile in the common SOL in the region on the high-field-side of the plasma. In this case the neutral atoms would travel freely until they came near the secondary separatrix where they would begin to ionise. In the common SOL the neutrals would have a nearly constant ionisation rate and their density would decay exponentially with a 1/e length approximately equal to the the ionisation mean-free-path. Since the D_α emissivity in the temperature range expected ($T_e \geq 5$ eV) has

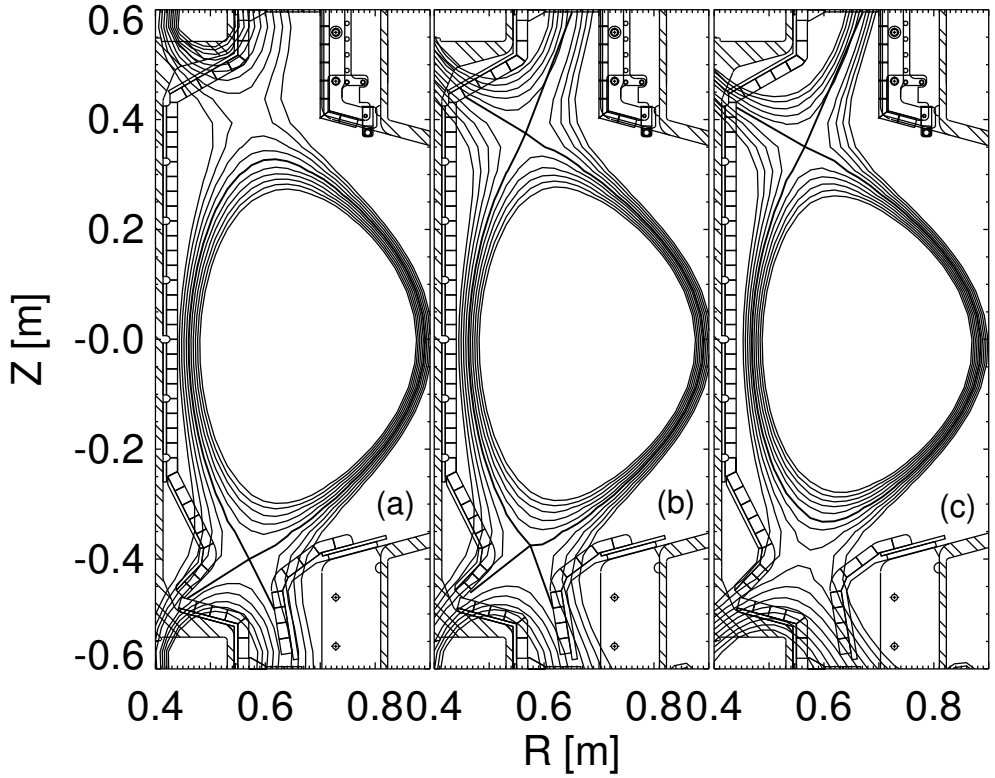

Figure 5. The three magnetic geometries that the plasma was scanned through to investigate the influence of the magnetic geometry on the D_α emission near the inner wall. Here (a) is a lower single null configuration, (b) is the double null configuration and (c) is the upper single null configuration.

a weak dependence on temperature and a linear dependence on both the electron and neutral density,

$$\epsilon_{D_\alpha} \propto n_e n_o, \tag{3}$$

the emissivity will depend on the plasma and neutral profiles. On the HFS of the emission peak the neutrals have a nearly flat density profile and therefore the HFS emission scale length is indicative of the electron density scale length. On the LFS of the emission peak the electron density varies more slowly and LFS emission scale length is governed by the neutral density. The peak in the emissivity occurs where the product of the electron and neutral densities are a maximum which occurs on the secondary separatrix.

A one dimensional space, two dimensional velocity, kinetic neutral code (KN1D) [8] was used to simulate the plasma-neutral interactions near the inner wall of the tokamak. This code requires as inputs the plasma profiles (temperature, density, and velocity) and the neutral pressure at the inner wall. KN1D uses many molecular and atomic processes to determine the distribution functions of both the atomic and molecular neutrals. The processes included are (1) charge exchange collisions, (2) electron-impact ionisation and dissociations, (3) elastic self-collisions (atomic and molecular), and (4) a variety of elastic cross-collisions (atom-ion, atom-molecule,

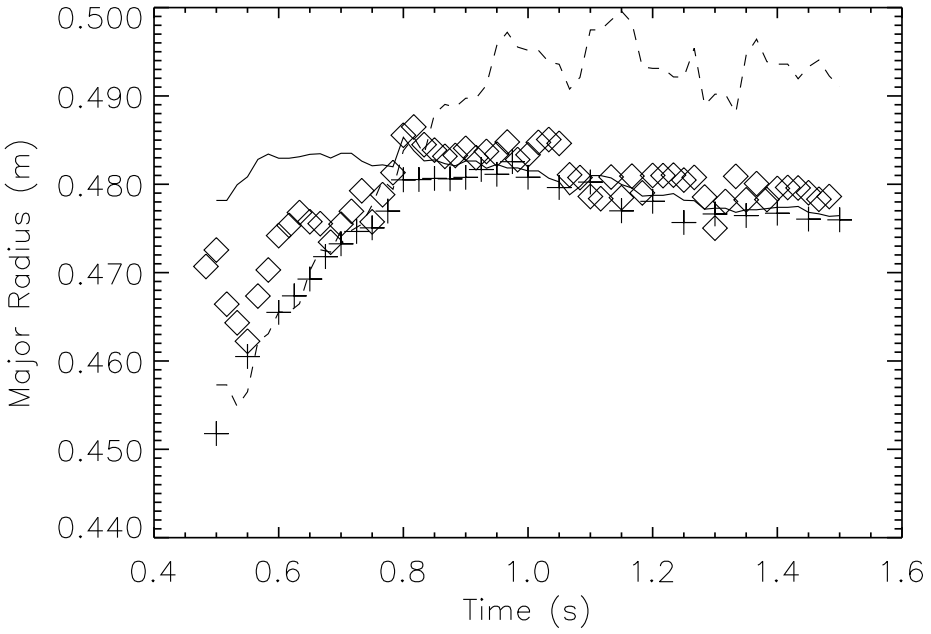

Figure 6. Plot showing the location of the peak in the emission from the observations (⋄) and the location of the peak in the emission from the kinetic neutral code KN1D (+) with respect to the location of the flux surface associated with the lower (–) and upper (- -) null for the inboard SOL.

molecule-ion).

The inputs used in simulating the inner wall SOL region included using typical plasma profiles in the common SOL, as measured on the LFS mid-plane by a scanning Langmuir probe, but with a sharp decay of the plasma density in the inner SOL (λ_n = 3 mm) beginning at the secondary separatrix. Using the LFS common SOL values for the plasma profile in the HFS common SOL is adequate since the LFS emission scale length in the KN1D output only changed by a few percent when the common SOL density profiles was varied from a flat density to a flat temperature profile while keeping pressure constant on a flux surface. The input value of the neutral molecular pressure at the inner wall is unimportant since the absolute scale of the KN1D output D_α emissivity is a linear function of this neutral pressure. When the neutral pressure at the inner wall was chosen to agree with the measured emissivity profile the pressures required were in the range of 0.6 to 3 mTorr.

The results of the simulations show an excellent agreement with the location of the emission peak (figure 6) and the LFS emission scale length (figure 8) and only a moderate agreement with the HFS emission scale length (figure 7). The location of the emission peak is typically where the electron density begins its steep decent toward the inner wall and the KN1D location of the emission peak is consistently below the emission peak location obtained from the camera data. This suggests that the plasma profiles used as input to KN1D should begin the sharp decay in plasma density slightly to the high field side of the secondary separatrix. The LFS emission

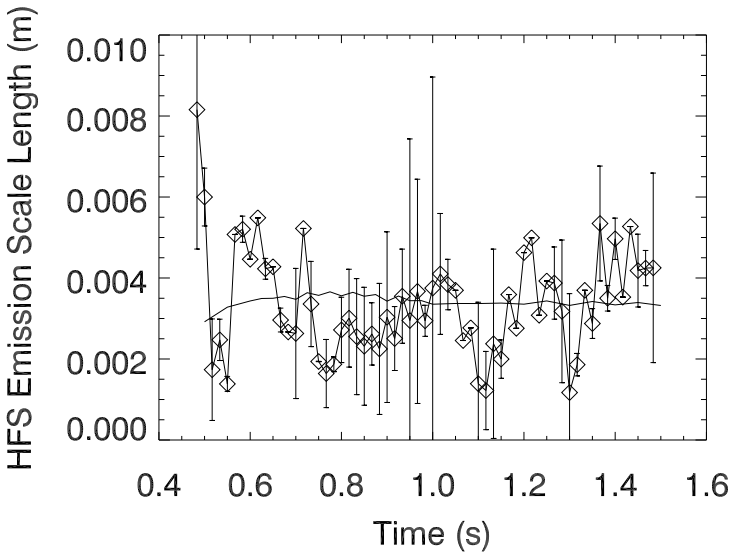

Figure 7. Plot showing the high-field-side emission scale length measured from the observations ($\diamond$) and the high-field-side emission scale length calculated from the kinetic neutral code KN1D (–) for the inboard SOL.

scale length decreases as the magnetic configuration nears double null (at 0.8 s). This decrease in scale length is due to the secondary separatrix approaching regions of higher density. The higher density yields a shorter ionisation mean-free-path for the neutrals and as described earlier a shorter emission scale length. The constancy of the HFS emission scale length is because the D_α emission profile on the HFS of the peak is dominated by the plasma density profile, which is given as an input to the code. Therefore, the LFS emission scale length result from the model could be made to match the measured result more closely. Since the constant value result is within the error bars for the measurement and little more information could be obtained by forcing the two results to match, the constant value result was seen as adequate. Figure 9 shows the $D_\alpha$emission profile for one modelled time slice varying the density scale length in the region between the secondary separatrix and the inner wall, showing that the strong density gradient beginning at the secondary separatrix is necessary to replicate the experimental observations. The three plasma density scale lengths used are (1) keeping the same plasma profile near the inner wall as is measured on the outboard side ($\lambda_- = 33.8$mm), (2) using a scale length that best matched the observed measurement ($\lambda_- = 3.5$mm), and (3) an intermediate value ($\lambda_- = 18.7$mm) to show the dependence of the solution on this scale length.

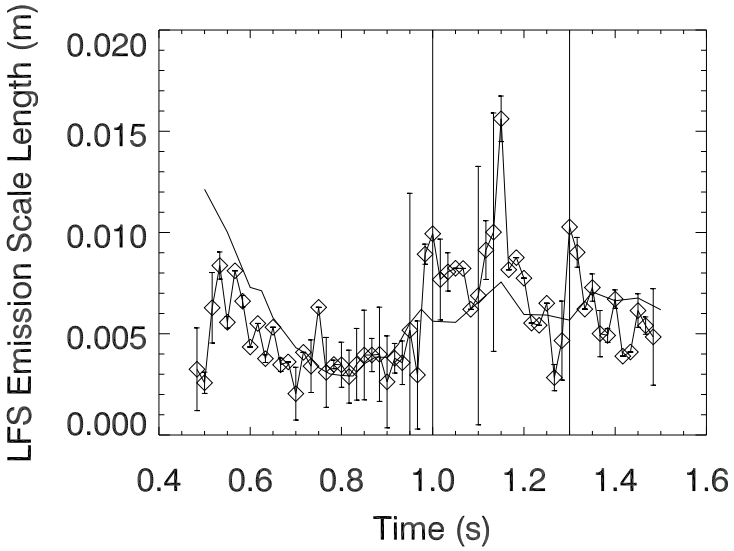

Figure 8. Plot showing the low-field-side emission scale length measured from the observations (⋄) and the low-field-side emission scale length calculated from the kinetic neutral code KN1D (–) for the inboard SOL.

4. Summary

Probe results show clear evidence that there is a steep density fall-off at the secondary separatrix in the high-field side SOL. These measurements show this steep decay begin a few millimetres toward the magnetic axis of the secondary separatrix, which is within the error of the secondary separatrix location reconstruction. In the steep fall-off region the plasma density decay length is ~ 1 mm when mapped to the outboard mid-plane.

Detailed measurements and analysis of D_α profiles at the inboard plasma edge also show a sharp density decay at the secondary separatrix. The density decay length in the inner SOL is ~ 0.8 mm when mapped to the outboard mid-plane, which is close to the Langmuir probe measured value of ~ 1 mm.

In addition, the D_α results show the dynamic behaviour when the magnetic equilibrium is scanned from lower single null through double null to upper single null. The HFS D_α emission scale length has no systematic dependence on the magnetic geometry, and the LFS D_α emission scale length decreases as the discharge approaches a double null configuration. Through interpretation of the neutral transport the location of the emission and the independence of the HFS emission scale length is explained by the sharp plasma density decay beginning at the secondary separatrix and decreasing toward the inner wall. The HFS emission scale length is a measure of

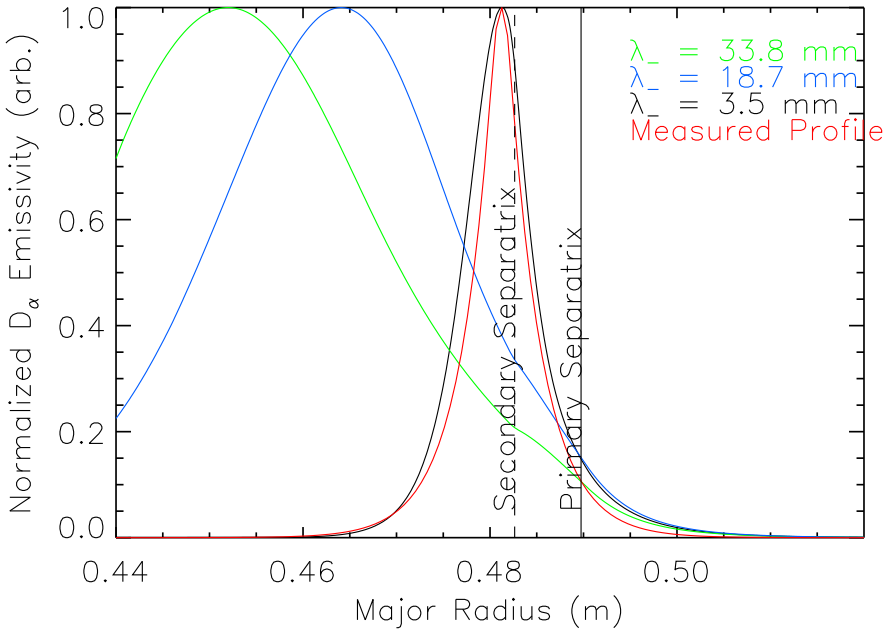

Figure 9. Plot of the D_α emission output from KN1D where the plasma density scale length is varied from 33.8 mm (the value if no change was made when compared to the outer SOL) to 3.5 mm (the best fit to the measured data) at the inboard SOL.

that plasma density decay length. The LFS emission scale length can be explained by the ionisation mean-free-path of the neutrals into the common SOL, and therefore is a measure of the fuelling efficiency, for the thermal neutrals moving toward the plasma from the secondary separatrix.

The existence of a sharp decay of the plasma density beginning at the secondary separatrix can explained by considering the typical SOL paradigm. In the SOL paradigm all plasma in the SOL flows along field lines to the divertor plate or limiter and the radial SOL plasma profiles are determined by this parallel transport. On the LFS of the common SOL and in the outboard SOL there is clear evidence that in some cases the perpendicular (radial) particle transport competes with or is larger than the parallel transport. This flattens the plasma profiles and is contrary to the typical SOL paradigm. [9, 10] In the HFS SOL, the profiles in the *common* SOL are set by the LFS dynamics, and in the inner SOL the profiles are more in line with the SOL paradigm. This explanation is consistent with the previous observations mentioned in section 1. The density decay length was shorter at the HFS of Alcator C because it was not connected to the LFS. The fluctuations measured at the inner wall on ASDEX, TEXT-U, and Alcator C-Mod during single-null discharges were the effect of the LFS dynamics on the HFS common SOL, while the lack of measured fluctuations during double-null discharges on ASDEX occurred because the inner SOL was not connected to the LFS and therefore was not influenced by the transport there.

References

[1] LaBombard B and Lipschultz B 1987 *Nucl. Fusion* **27** 81
[2] Endler M *et al* 1995 *Nucl. Fusion* **35** 1307
[3] Hurwitz P D 1995 *Optical Imaging of Turbulence Fluctuations in the Texas Experimental Tokamak-Upgrade* [dissertation] University of Texas at Austin
[4] Terry J L *et al* 2003 *Phys. Plasmas* **10** 1739
[5] Pitcher C S *et al* 1993 *Proceedings of the 20th EPS Conference on Controlled Fusion and Plasma Physics* (European Physical Society) **17C** 291
[6] Pitcher C S *et al Rev. Sci. Instrum.* **72** 103
[7] Boswell C, Terry J L, Lipschultz B, and Stillerman J 2001 *Rev. Sci. Instrum.* **72** 935
[8] LaBombard B 2001 *Plasma Science and Fusion Center Research Report* PSFC-RR-01-3
[9] LaBombard B *et al* 2000 *Nucl. Fusion* **40** 2041
[10] LaBombard B *et al* 2001 *Phys. Plasmas* **8** 2107